UDC 54.057:547.83:547.792
DOI: 10.15587/2519-4852.2025.337951

TARGETED STRUCTURAL DESIGN OF MOLECULAR SCAFFOLDS FOR DUAL-ACTION PEPTIDOMIMETIC INHIBITORS AGAINST SARS-COV-2 M^{PRO} AND PL^{PRO}

Larysa Yevsieieva, Alexander Kyrychenko, Pavlo Trostianko, Volodymyr Ivanov, Sergiy M. Kovalenko, Oleg Kalugin

The two proteases of SARS-CoV-2 coronavirus – the main protease (M^{pro} or $3CL^{pro}$) and the papain-like protease (PL^{pro}) – are essential enzymes required for the successful replication of the virus within cells. Both proteases have become major targets in the development of antiviral drugs against SARS-CoV-2. The potential to achieve a dual inhibitory effect has sparked significant interest in creating dual inhibitors as complex therapeutic agents for this virus. In this article, we discuss the development and in silico evaluation of a series of new peptidomimetic molecules designed as dual-action inhibitors of both SARS-CoV-2 M^{pro} and PL^{pro}, along with their synthesis. We implemented a combined approach that began with developing a basic molecular model, considering the substrate specificity of the active centers of each protease. Through rational in silico design, we created a series of peptidomimetics. Further analysis of how these compounds bound to the active sites of both proteases enabled us to identify several new structural hits, including hydantoin derivatives, as potential dual inhibitors of M^{pro} and PL^{pro}.

The aim of the study. *This study aims to establish a common molecular framework for designing dual-action inhibitors targeting the SARS-CoV-2 M^{pro} and PL^{pro} proteases. The research includes receptor-oriented molecular docking, in silico optimization, and the selection and synthesis of the most active candidate structures for further in vitro experimental studies.*

Materials and methods. *LigandScout 4.5 software is used for 3D pharmacophore analysis, visualization, and molecular docking. AutoDock Vina 1.1 provides tools for molecular docking. The PLIP (Protein-Ligand Interaction Profiler) web servers are utilized to study molecular binding mechanisms. DataWarrior 6.0 software helps create a library of molecular structures, calculate physicochemical properties, and analyze molecular frameworks. SwissADME web server is used to predict ADME parameters and assess the pharmacokinetic properties of small molecules as potential drugs.*

Results. *We analyzed the substrate specificity of the binding sites of the M^{pro} and PL^{pro} proteases, which enabled us to identify a common amino acid sequence containing shared recognition elements for both proteases. By rationally modifying the functional groups in this initial base structure, utilizing the principle of isosteric replacement and incorporating non-classical bioisosteres, we developed a series of peptidomimetic frameworks. Molecular docking conducted at the active sites of both M^{pro} and PL^{pro}, along with the assessment of their binding energy values (in kcal/mol), identified several structures with potential for dual inhibition. Notably, hydantoin derivatives demonstrated the strongest binding affinity to the active sites of both proteases.*

Conclusions*. We have identified promising peptidomimetic molecular structures that demonstrate dual inhibitory activity against the SARS-CoV-2 proteases through in silico analysis. Specifically, we discovered a novel class of hydantoin derivatives that act as inhibitors for both SARS-CoV-2 M^{pro} and PL^{pro}. The synthesis methods we developed allow for the preparation of these compounds for further in vitro studies*

Keywords*: SARS-CoV-2, M^{pro} protease, PL^{pro} protease, peptidomimetics, dual inhibitors, molecular docking*

How to cite:
Yevsieieva, L., Kyrychenko, A., Trostianko, P., Ivanov, V., Kovalenko, S. M., Kalugin, O. (2025). Targeted structural design of molecular scaffolds for dual-action peptidomimetic inhibitors against SARS-CoV-2 M^{PRO} and PL^{PRO}. ScienceRise: Pharmaceutical Science, 5 (57), 56–67. http://doi.org/10.15587/2519-4852.2025.337951

1. Introduction

The main protease (M^{pro}) and papain-like protease (PL^{pro}) of the SARS-CoV-2 coronavirus are crucial for its replication. Inhibiting the activity of these proteases hinders the post-translational processing of viral polyproteins [1]. This disruption prevents the formation of functional viral proteins, ultimately leading to the virus's inability to replicate within the host cell [2].

Both M^{pro} and PL^{pro} are cysteine proteases, which, however, differ in substrate specificity and the topology of their active sites. The catalytic center of SARS-CoV-2 M^{pro}, which is crucial for the protease's biological activity, contains a catalytic dyad made up of histidine and cysteine residues (His 41 and Cys145). This dyad is located within a hydrophobic cavity that forms the substrate-binding pocket [3]. Covalent inhibitors of M^{pro} specifically target the nucleophilic thiol residue Cys145, forming a covalent bond with it. In contrast, the catalytic triad of PL^{pro} is situated at the junction of its two main domains and comprises the residues Asp286, His272, and Cys111 [4, 5]. The active

site of the SARS-CoV-2 PL^{pro} protease is situated within a hydrophobic pocket of the molecule. However, its shape is more complex, which studies suggest may lead to stoichiometric challenges for the effective covalent interaction between the inhibitor and the catalytic cysteine, Cys111, found in the active site [6].

The development of inhibitors targeting the M^{pro} and PL^{pro} proteases is one of the most promising strategies in the search for effective drugs against the SARS-CoV-2 virus [7]. A peptidomimetic approach has been widely utilized to create covalent inhibitors of these proteases. By studying the substrate specificity of the proteases, researchers have developed several foundational structures that mimic the highly conserved amino acid sequences found in the natural substrates recognized by the corresponding proteases. However, peptide inhibitors have several pharmacokinetic limitations when used directly. They are prone to hydrolysis of their peptide bonds, resulting in metabolic instability. Additionally, they do not effectively penetrate cell membranes. This lack of stability for small peptides *in vivo* has led to the development and use of peptidomimetics [4].

The development of peptidomimetics – compounds that replicate the essential structural and pharmacophore elements of peptide ligands needed for interaction with enzymes – is a promising avenue for designing new biologically active molecules [8]. These compounds can potentially offer enhanced pharmacokinetic properties, increased conformational rigidity, and better stability *in vivo*, all while maintaining their ability to interact effectively with target proteins.

The rational design strategy for the basic structure of a covalent inhibitor, as proposed in [9], consists of two key stages:

a) identifying a suitable chemical framework (template) that can effectively interact with the target enzyme;

b) designing the main functional groups and the covalently reactive group in a way that promotes specific interaction with the enzyme's active site [10].

To develop peptidomimetics that mimic the natural substrates of viral proteases, it is essential to understand the specific amino acid sequences recognized by M^{pro} and PL^{pro}.

The main protease M^{pro} of SARS-CoV-2 exhibits strict substrate specificity and targets the recognition sequence Leu-Gln↓Gly (Ser, Ala), where the arrow (↓) indicates the cleavage site [1, 11]. A key feature of this site is the presence of the amino acid glutamine (Gln) followed by a small amino acid, typically serine (Ser), alanine (Ala), or glycine (Gly). One notable characteristic of the SARS-CoV-2 M^{pro} protease, compared to human proteases, is its ability to specifically cleave peptides after the glutamine residue. This highly conserved tripeptide sequence recognized by M^{pro} serves as the primary template for the rational design of peptidomimetic inhibitors. This design approach ensures that these inhibitors exhibit both specificity and high affinity for the viral protease (Fig. 1).

One of the first efficient peptidomimetic inhibitors to show potential against the protease M^{pro} of coronaviruses is GC376. This compound was initially developed to inhibit the SARS-CoV-1 virus, and its effectiveness against SARS-CoV-2 M^{pro} was later confirmed in in vitro experimental studies [12]. Another peptidomimetic inhibitor, N3, also demonstrated high inhibitory efficacy against SARS-CoV-2 M^{pro} [13]. These compounds contain an analogue of the tripeptide sequence associated with M^{pro} substrate recognition (Fig. 2), ensuring specific and high-affinity binding in the enzyme's active site.

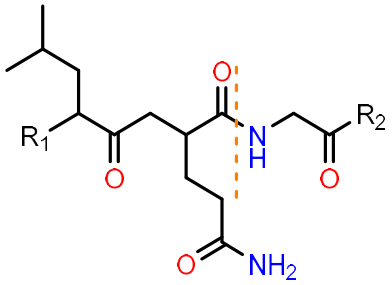

Fig. 1. *M^{pro}* recognition tripeptide sequence: Leu-Gln↓Gly, where R_1 and R_2 are continuations of the polypeptide chain, and the dash line is the cleavage site

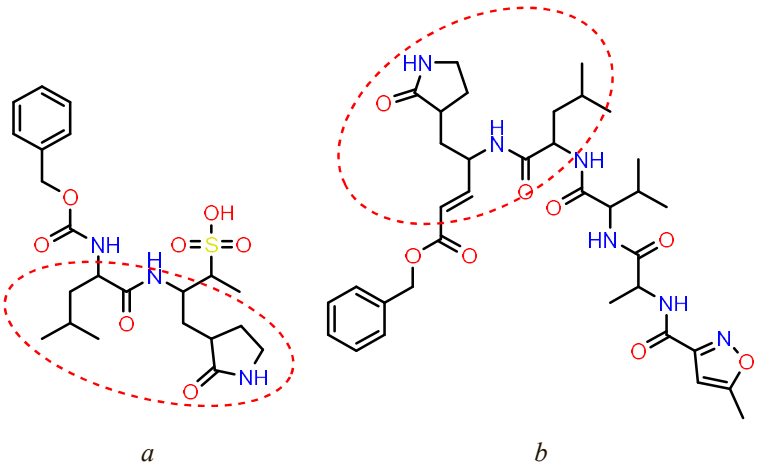

a *b*

Fig. 2. Peptidomimetic inhibitors of *M^{pro}* protease: *a* – ligand GC376 (PDB: 6L70); *b* – ligand N3 (PDB:5EU8), isolated fragment – analogue of the tripeptide sequence of *M^{pro}* substrate recognition

This approach, which focuses on the rational design of amino acid sequences for substrate recognition and follows the principles of isosteric replacement, has become fundamental in the development of many peptidomimetic inhibitors. This includes the clinically approved M^{pro} inhibitor, nirmatrelvir (Paxlovid) [14, 15]. Currently, the most prominent and widely researched mechanism of action for M^{pro} inhibitors involves a covalent interaction with the enzyme. The effectiveness of the covalent M^{pro} inhibitor relies on the formation of a covalent bond between the ligand being developed and the nucleophilic residue Cys145 located in the active site of the protease. To achieve this, the peptidomimetic framework of M^{pro} inhibitors must include an active electro-

philic group that facilitates the covalent modification of M^{pro}. Electrophilic groups generally include classical Michael acceptors (MAs) as well as activated carbonyl derivatives, such as alpha-ketoamides and aldehydes. MAs can lead to covalent and irreversible inhibition of enzymes. In theory, irreversible inhibitors have the potential to completely neutralize biomolecular targets if there is sufficient exposure time [16]. However, it is important to note that irreversible inhibition may pose a risk of toxicological consequences due to its cumulative effects [17, 18]. Currently, irreversible inhibitors targeting the thiol group of cysteine proteases are primarily utilized as anticancer drugs. In contrast, reversible covalent inhibitors are often preferred in other therapeutic areas. These compounds typically feature less electrophilic groups, allowing them to form reversible covalent adducts with the active sites of biological targets [19]. Examples of clinically approved reversible covalent inhibitors of protein kinases and proteases that are successfully used in medical practice include Boceprevir, Narlaprevir, and Nirmatrelvir (Fig. 3).

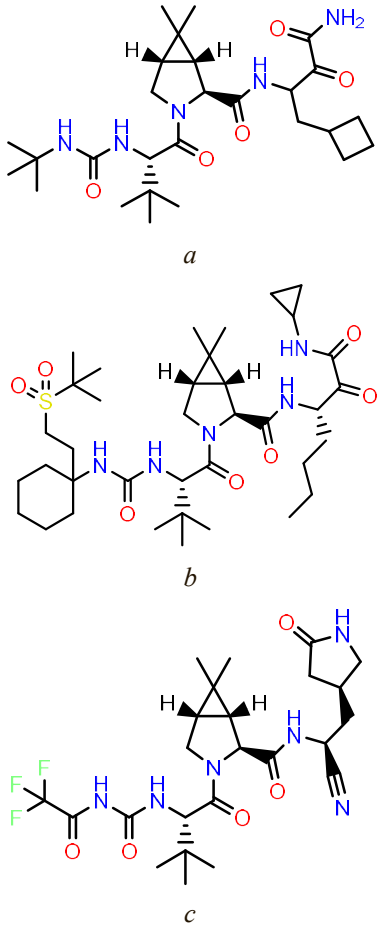

Fig. 3. Structures of reversible covalent inhibitors of protein kinases and proteases approved as drugs: *a* – *Boceprevir,* a hepatitis C virus protease inhibitor [20]; *b* – *Narlaprevir,* a hepatitis C virus protease inhibitor [21]; *c* – *Nirmatrelvir,* an inhibitor of the SARS-CoV-2 M^{pro} protease [22]

The papain-like protease (PL^{pro}) of SARS-CoV-2 specifically recognizes and cleaves the tetrapeptide sequence Leu-X-Gly-Gly, where "X" represents any amino acid [1, 23, 24]. The arrow (↓) indicates the site of peptide bond hydrolysis, which occurs on the carboxyl side of the last glycine [25]. This cleavage results in the release of non-structural proteins that are essential for viral replication [26, 27]. During research aimed at identifying PL^{pro} protease inhibitors, VIR250 and VIR251 were among the first notable peptidomimetic compounds to show inhibitory potential. These inhibitors were designed based on a specific enzyme recognition sequence and served as foundational structures for the rational development of more bioavailable inhibitors [28]. Despite the advantages of covalent inhibition, most research has concentrated on the development of non-covalent PL^{pro} inhibitors [6]. The non-covalent ligand GRL0617 and its analogues currently represent the primary PL^{pro} inhibitors with a confirmed mechanism of action [23] (Fig. 4).

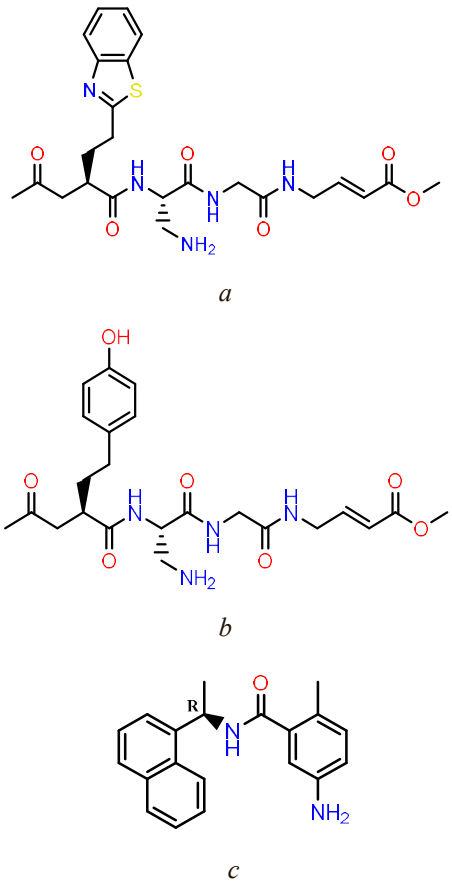

Fig. 4. Peptidomimetic covalent inhibitors *PL^{pro}* VIR250 and VIR251, non-covalent inhibitor *PL^{pro}* GRL0617: *a* – VIR250 covalent inhibitor of *PL^{pro}*; *b* – VIR251 covalent inhibitor of *PL^{pro}*; *c* – GRL0617 non-covalent inhibitor of *PL^{pro}* [4]

Research into covalent inhibitors of PL^{pro} is making significant progress [23, 25, 29]. Recent developments focus on peptidomimetic inhibitors that covalently target the SARS-CoV-2 PL^{pro} enzyme and effectively inhibit its activity [30]. Studies have confirmed that these inhibitors can form a covalent bond with the catalytic residue cysteine 111 (Cys111) located in the enzyme's active site [30].

The development of dual inhibitors targeting both M^{pro} and PL^{pro} is a crucial and strategically important area of research in the fight against coronavirus infections [31, 32]. The concept of "polypharmacology" suggests that moderately inhibiting multiple targets may be more effective and less susceptible to resistance than strongly inhibiting a single target. Additionally, even weak inhibition of a second target can produce a synergistic effect, resulting in a significant overall antiviral impact [33]. While developing covalent inhibitors for PL^{pro} presents certain challenges, creating a dual inhibitor that effectively targets M^{pro} (where covalent inhibition is more well-established) and significantly affects PL^{pro} may be an attainable objective.

2. Planning (methodology) of the study

The study commenced with an analysis of the substrate specificity of the M^{pro} and PL^{pro} proteases to establish the overall amino acid sequence. This sequence served as the foundation for the structure-oriented design of peptidomimetic inhibitors. By applying the principles of isosteric replacement, we developed several initial frameworks. We then selected the most promising structures through molecular docking, starting with those that exhibited stronger binding than co-crystallized ligands and subsequently identifying those that showed high affinity for both proteases [7]. The selection process for the strongest dual-binding structures, along with an analysis of their potential and rational pathways for their synthesis, enabled us to develop and synthesize a small library of compounds for further in vitro studies.

3. Materials and methods

A series of three-dimensional X-ray crystal structures of target proteins – SARS-CoV-2 proteases – were obtained from the Protein Data Bank and used for receptor-based docking, as summarized in Table 1.

Table 1

M^{pro} and *PL^{pro}* structures from the Protein Data Bank in complex with covalent peptidomimetic inhibitors used in the study

No.	PDB	Description
1	6M0K	The crystal structure of COVID-19 main protease *M^{pro}* in complex with an inhibitor 11b
2	7UUP	SARS-CoV-2 Main protease *M^{pro}* in complex with Nirmatrelvir (PF-07321332). Due to the clinical significance of Nirmatrelvir, this model is often used for comparison and development of new covalent inhibitors
3	7TGR	Structure of SARS-CoV-2 main protease *M^{pro}* in complex with GC376
4	7JPZ	Structure of the SARS-CoV-2 main protease *M^{pro}* in complex with inhibitor MPI1
5	8EUA	Structure of SARS-CoV-2 *PL^{pro}* bound to a covalent inhibitor
6	8IHO	Crystal structures of SARS-CoV-2 papain-like protease *PL^{pro}* in complex with covalent inhibitors
7	7LFU	Crystal structure of the SARS-CoV-1 Papain-like protease *PL^{pro}* in complex with peptide inhibitor VIR250
8	9DO5	SARS-CoV-2 papain-like protease (*PL^{pro}*) with inhibitor Jun12665

DataWarrior 6.0 software [34] was used to create a library of molecular structures, calculate physicochemical properties, and analyze molecular frameworks.

Molecular docking calculations were performed using LigandScout 4.5 [35] and AutoDock Vina 1.1 [36, 37].

The reagents used in this work were manufactured by Sigma-Aldrich (USA) and were purified using standard techniques. Control of the reactions was monitored using thin-layer chromatography on "Supelco TLC Silica gel 60 F_{254}" plates with an eluent of ethyl acetate-hexane (1:2 ratio). ^{1}H NMR spectra were recorded on Varian Gemini 400 MHz spectrometers using dimethyl sulfoxide (DMSO-d6) as the solvent. LC/MS spectra were recorded using a PE SCIEX API 150EX liquid chromatograph equipped with a UV detector (λ_{max} 215 and 254 nm) and a Luna-C18 column, Phenomenex (100 × 4 mm). Elution started with water and ended with acetonitrile/water (95:5, v/v) using a linear gradient at a flow rate of 0.15 mL/min and an analysis cycle time of 25 min.

4. Research result

4. 1. Rational design of a dual inhibitor of M^{pro} and PL^{pro} *in silico*

Our research into the development of peptidomimetics as dual inhibitors of SARS-CoV-2 proteases M^{pro} and PL^{pro} began with a comprehensive analysis of the substrate specificity of both proteases. To identify the ideal scaffold capable of simultaneously inhibiting both proteases, we conducted a comparative analysis of the specific amino acid sequences that M^{pro} and PL^{pro} recognize.

In our study, we focused on M^{pro} from SARS-CoV-2, which specifically cleaves the sequence Leu-Gln↓(Gly/Ser/Ala). We also noted that PL^{pro} recognizes the tetrapeptide sequence Leu-X-Gly-Gly↓, where X represents a variable amino acid. To enhance our model, we proposed introducing a glutamine (Gln) residue at position X, similar to the Gln residue found in the M^{pro} substrate. Consequently, the initial tetrapeptide sequence for our design became Leu-Gln-Gly-Gly (as shown in Fig. 5). This strategy aims to create a single peptidomimetic scaffold that can effectively interact with the active sites of both proteases by utilizing their common or adapted recognition elements.

We chose the polypeptide backbone of the tetrapeptide Leu-Gln-Gly-Gly as the foundation for developing a dual peptidomimetic inhibitor that targets the active sites of both SARS-CoV-2 M^{pro} and PL^{pro} proteases.

We initiated our search for the optimal peptidomimetic base structure derived from the original tetrapeptide Leu-Gln-Gly-Gly by specifically modifying the side chains of its amino acid residues (Fig. 6).

We applied the principle of isosteric replacement, which involves altering the functional groups in a base molecule using non-classical bioisosteres. The primary objective of this substitution was to create a peptidomimetic molecule that reduces the metabolic lability of

peptide bonds, thereby improving in vivo stability while preserving the pharmacological profile.

Non-classical bioisosteres can mimic the spatial arrangement, electronic properties, and other crucial physicochemical characteristics of functional groups that are essential for interaction with biological targets. By utilizing isosteric replacement, we aim not only to enhance potential biological activity and stability but also to optimize the pharmacokinetic profile of the molecule as a potential drug substance [38].

The leucine residue (Leu, position P1 in Fig. 6) is a significant part of the recognizable substrate polypeptide chain in both proteases, M^{pro} and PL^{pro}. It plays a crucial role in facilitating hydrophobic interactions within the enzyme's active site. To enhance conformational rigidity and improve binding, we modified the leucine side chain by substituting it with a cyclic hydrophobic element. Cyclic analogues tend to provide a more stable conformation compared to their linear counterparts, which could potentially enhance both binding affinity and selectivity.

Glycine residues (Gly) in the P3 and P4 positions (as shown in Fig. 6) lack a side chain, which increases the lability and mobility of the polypeptide chain. Glycine is commonly used in regions of the protein chain that require maximum curvature [19]. In the development of the peptidomimetic, we replaced the glycine residue at the P4 position with either a cyclic or heterocyclic element, which may or may not contain a double bond with an oxygen atom.

The side chain of glutamine (marked P2 in Fig. 6) contains an amide group that can function as either a proton donor or acceptor. This amide group is essential for its interaction with the enzyme's active site, facilitating bond breaking or formation. In developing the peptidomimetic, we replaced the glutamine side chain in the basic structure of the teppepetide with structurally similar non-classical bioisosteric fragments. This change was made to maintain key interactions while enhancing the stability of the molecule [39].

Based on these assumptions, we developed a series of peptidomimetic structures through rational modifications of the functional groups in the initial tetrapeptide sequence Leu-Gln-Gly-Gly. The purpose of these modifications was to identify potential dual covalent inhibitors of SARS-CoV-2 proteases (Fig. 7).

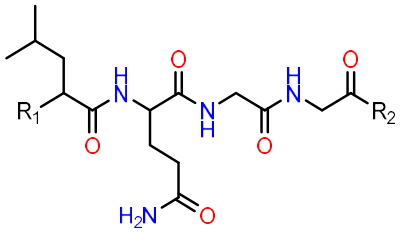

Fig. 5. The tetrapeptide recognition sequence *PL*^{pro}: Leu-X-Gly-Gly, where X is Gln, and R_1 and R_2 are continuations of the polypeptide chain

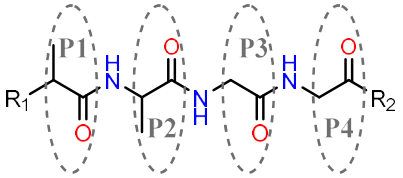

Fig. 6. The labels P1, P2, P3, and P4 are parts of the tetrapeptide Leu-Gln-Gly-Gly corresponding to amino acid residues with corresponding side chains that may have chemical analogues. In the case of P3 and P4, this is the part of the tetrapeptide containing glycine residues, which have no side chains

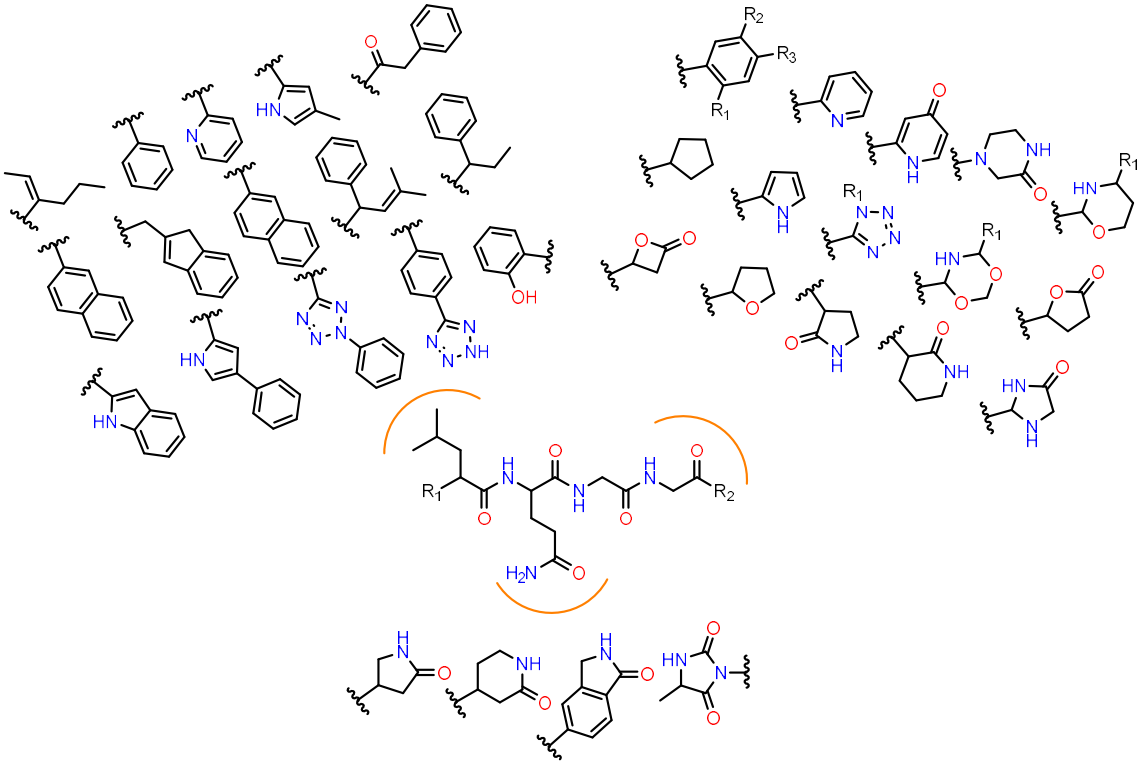

Fig. 7. Design of peptidomimetics based from the structure of the Leu-Gln-Gly-Gly tetrapeptide

To identify the most promising compounds, we utilized molecular docking to assess their potential interactions with the active sites of both SARS-CoV-2 proteases, M^{pro} and PL^{pro}. Molecular docking was conducted using the corresponding target structures for M^{pro} and PL^{pro} (refer to Table 1). The results of the docking process allowed us to rank the molecules based on their binding energies.

In the initial stage, we selected compounds that exhibited binding energies equal to or greater than those of the co-crystallized reference ligand for each protease. From this subset, we then identified the molecules that showed strong binding affinity to both enzymes. Ultimately, we selected eight compounds that demonstrated the highest binding affinity for both proteases (Fig. 8). These peptidomimetic structures display significant affinity for the active sites of both M^{pro} and PL^{pro} in SARS-CoV-2 (refer to Table 2).

All the selected hit molecules listed in Table 2 exhibited strong interactions with the substrate-binding pockets of SARS-CoV-2 M^{pro}, with binding energy values ranging from –7.3 to –8.7 kcal/mol. For several of these compounds, the binding energy values were even more favorable than those of co-crystallized ligands, which are recognized and validated inhibitors of SARS-CoV-2 M^{pro}. Similarly, all hit molecules from Table 2 demonstrated robust interactions with the substrate-binding pocket of SARS-CoV-2 PL^{pro}, with docking energy values between –7.3 and –9.8 kcal/mol. For certain molecules, the binding energies were greater than those of co-crystallized ligands that are known inhibitors of SARS-CoV-2 PL^{pro}. Among all the compounds studied, HIT6, a hydantoin derivative, exhibited the strongest binding to the active sites of both proteases. In this context, the hydantoin fragment is believed to form a covalent interaction with the key catalytic residue Cys145 in the M^{pro} active site.

Based on the basic structure of the peptidomimetic HIT6 (hydantoin derivative), we created a small library of compounds with similar chemical functions and high potential for synthesis (Fig. 9).

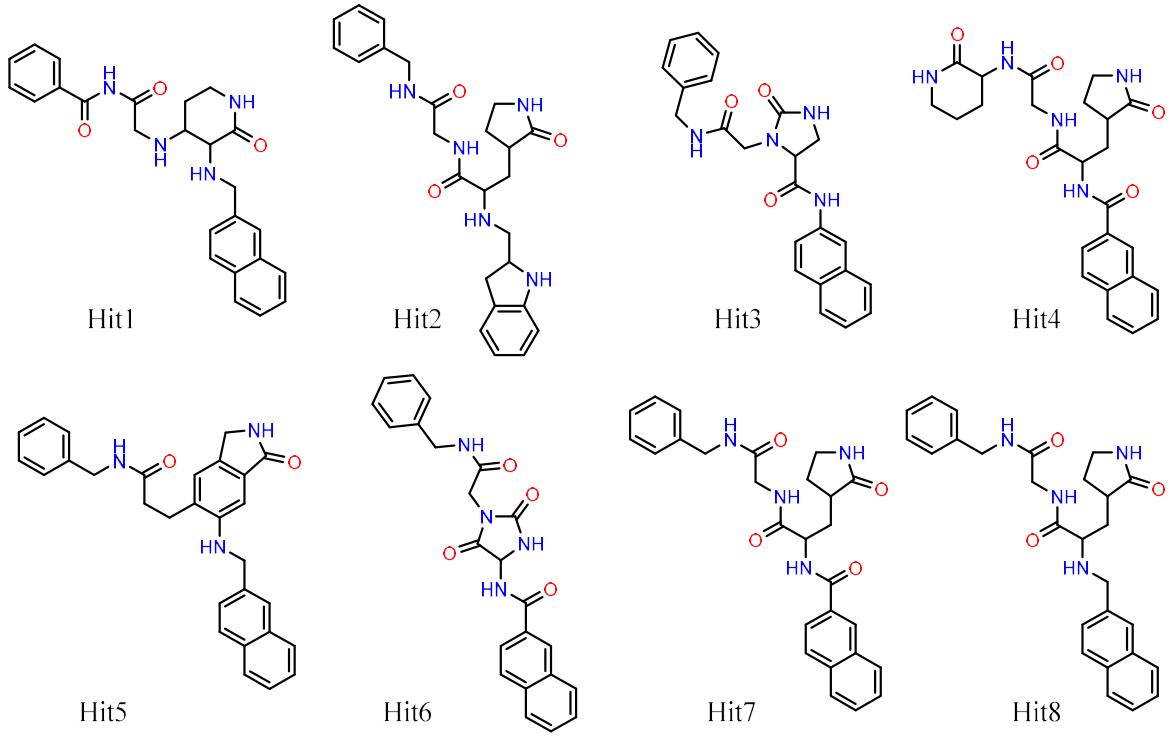

Fig. 8. Compounds showing the best binding affinity with the active sites of the both proteases

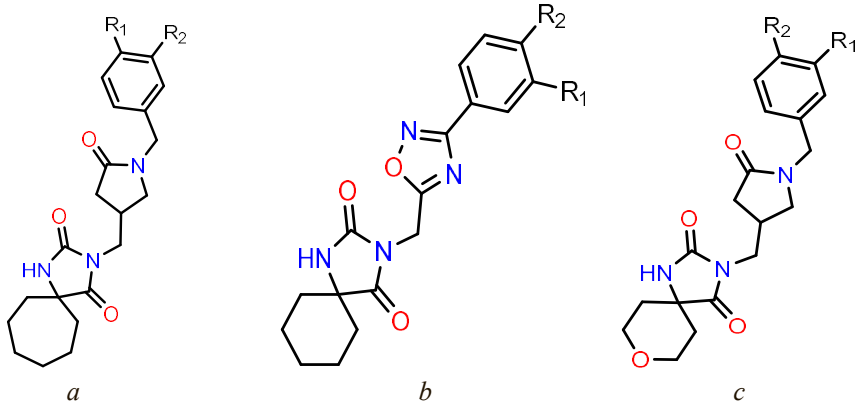

Fig. 9. General structure of the chosen scaffolds: *a–c* – show three scaffolds of compounds from the developed library of hydantoin derivatives

Molecular docking calculations revealed a number of optimized analogues of HIT6 (Fig. 10) demonstrating significant affinity for the active sites of both proteases (Table 3).

The absorption, distribution, metabolism, and excretion (*in silico* ADME) profiles of the investigated derivatives suggest that they possess favorable pharmacokinetic properties, making them potential drug candidates. All the molecules fall within the optimal range of physicochemical properties required for drug substances: lipophilicity measured by xlogP ranges from –0.7 to +5.0, molecular weight (M_w) ranges from 150 to 500 g/mol, polar surface area (TPSA) ranges from 20 to 130 Å^2, and solubility (as indicated by *c*log*S*) does not exceed 6 (refer to Table 4). Furthermore, all molecules meet the following criteria: structural saturation, with carbon atoms in sp^3 hybridization at a minimum of 0.25, and flexibility, which is limited to no more than 9 rotational bonds.

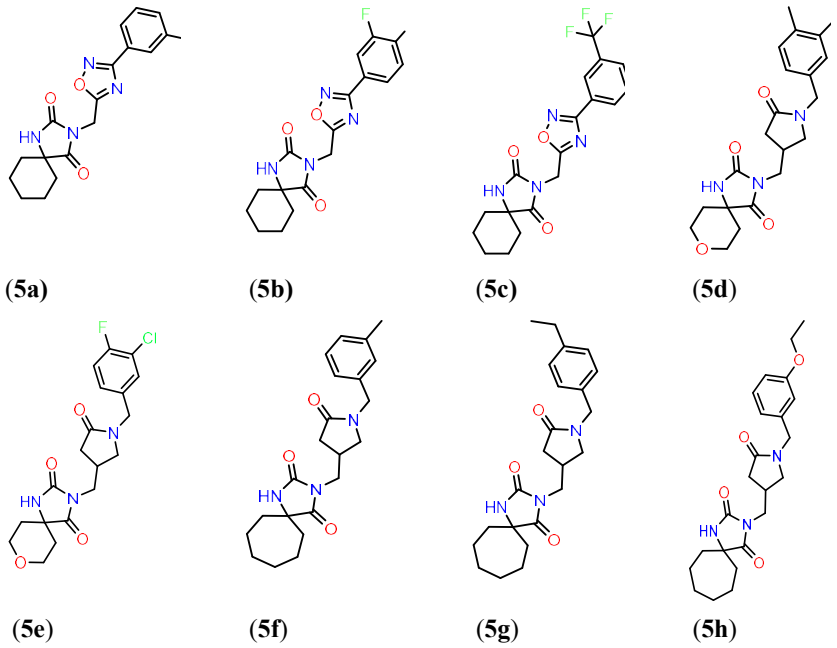

Fig. 10. Compounds from the developed library of hydantoin derivatives that showed the best binding affinity with the active sites of both proteases

Table 2

Molecular docking results: binding energies of hit molecules with active sites of SARS-CoV-2 *M*^{pro} and *PL*^{pro} proteases

Target	REF*	Hit1	Hit2	Hit3	Hit4	Hit5	Hit6	Hit7	Hit8
M^{pro}									
6M0K	–7.5	**–8.0**	**–7.9**	**–7.7**	–7.4	**–7.6**	**–7.7**	**–7.5**	**–7.6**
7UUP	–8.2	–8.0	–7.9	**–8.5**	–7.7	**–8.2**	**–8.2**	**–8.2**	–7.6
7TGR	–7.4	–7.3	**–8.6**	**–8.0**	**–8.3**	**–8.7**	**–8.1**	–7.3	–7.3
7FAZ	–8.3	–7.5	**–8.3**	–7.4	–8.0	–7.6	**–8.3**	–8.0	–8.0
PL^{pro}									
8EUA	–8.3	**–8.7**	**–8.7**	**–8.3**	–8.1	**–9.5**	**–9.6**	**–8.6**	–8.0
8IHO	–8.6	–7.5	–7.6	**–9.5**	**–8.7**	**–8.6**	**–9.8**	**–9.6**	**–9.3**
7LFU	–7.4	–7.3	**–7.6**	–7.2	–7.4	–7.2	**–7.8**	–7.3	**–7.5**
9D05	–8.4	–8.3	**–8.6**	**–8.7**	–8.4	–8.2	**–9.1**	–8.2	–8.2

Table 3

Molecular docking results: binding energies of hit molecules from the developed library of hydantoin derivatives with the active sites of SARS-CoV-2 M^{pro} and PL^{pro} proteases

Target	REF*	5a	5b	5c	5d	**5e**	**5f**	**5g**	**5h**
M^{pro}									
6M0K	–7.6	–7.6	**–7.8**	–7.5	**–7.7**	–7.5	**–7.7**	–7.4	–7.4
7UUP	–8.2	–7.9	**–8.3**	–7.7	–7.9	–7.9	**–8.5**	–8.1	–7.7
7TGR	–7.2	**–8.2**	**–8.2**	**–8.0**	**–9.2**	**–8.3**	**–7.8**	**–8.2**	–7.4
7FAZ	–8.2	**–8.6**	**–8.6**	–8.2	**–8.8**	**–8.4**	–7.8	–8.3	–7.8
7MB2	–7.7	**–9.2**	**–8.5**	**–8.6**	**–8.9**	**–8.5**	**–8.5**	–7.7	**–8.4**
PL^{pro}									
8EUA	–8.7	–8.3	–8.7	**–9.4**	**–9.0**	–8.6	–7.5	**–8.8**	–7.8
8IHO	–8.8	**–9.2**	**–9.0**	**–9.7**	**–9.6**	**–9.2**	–8.6	**–9.6**	–8.5
7LFU	–8.5	**–9.0**	**–8.7**	**–8.6**	**–8.9**	–8.3	**–9.3**	–7.8	**–9.3**
9D05	–8.4	–7.9	–8.0	–8.3	**–8.7**	–8.7	–7.7	–7.5	–7.5

*Note: * – the reference co-crystalized ligand from the corresponding PDB structure.*

A preliminary *in silico* assessment of the pharmacokinetic profile of new molecules using the SwissADME web server provides vital criteria for evaluating their potential as drugs. Key parameters of a drug's pharmacokinetic profile summarize ADME properties in Table 4. Conducting early ADME assessments during the optimization phase of promising hit molecules can significantly reduce the likelihood of negative results in subsequent in vitro and in vivo testing. The pharmacokinetic assessment available on the SwissADME web server includes several molecular characteristics: passive absorption in the gastrointestinal tract (HIA), penetration through the blood-brain barrier (BBB), and binding to transport proteins such as P-glycoprotein (PGP), which play a crucial role in drug elimination from the body (Table 4).

Our preliminary evaluation of the hit molecules from the developed library of hydantoin derivatives showed a favorable pharmacokinetic profile for all compounds. Each molecule demonstrated good absorption in the gastrointestinal tract (high intestinal absorption, or HIA+). Notably, two molecules, ***5f*** and ***5g***, appear to cross the blood-brain barrier. This characteristic may lead to potential unwanted side effects on the central nervous system (CNS), depending on the therapeutic objectives. Additionally, all molecules displayed binding to transport proteins, which facilitates their elimination from the body and suggests a reduced risk of accumulation.

Overall, this study highlights the potential of the developed peptidomimetics, particularly hydantoin derivatives, as dual inhibitors of SARS-CoV-2 proteases.

Table 4

Physicochemical properties and *in silico* ADME characteristics for hit molecules from the developed library of hydantoin derivatives.

Ligand	*c*Log*S*	Molecular weight (g/mol)	*c*Log*P*	Polar surface area (Å²)	HIA*	BBB*	PGP*
5a	–4.3	340.4	2.1	88.3	+	–	+
5b	–4.6	362.3	1.9	88.3	+	–	+
5c	–4.8	394.4	2.6	88.3	+	–	+
5d	–2.9	385.5	1.2	79.0	+	–	+
5e	–3.2	409.8	1.2	79.0	+	–	+
5f	–3.7	383.5	2.4	69.7	+	+	+
5g	–3.8	397.5	2.8	69.7	+	+	+
5h	–3.6	413.5	2.4	79.0	+	–	+

*Note: * HIA – penetration through the gastrointestinal tract wall; BBB – penetration through the blood-brain barrier; PGP – binding to transport proteins that ensure the elimination of the drug substance from the body.*

4. 2. Chemical library synthesis

Spyhydatoins **3a-c** were obtained by Bucherer-Bergs reaction [40] (Fig. 11) from corresponding ketones **1a-c** [41, 42]. Acetone cyanohydrin **2** was used as an alternative to potassium or sodium cyanide [43, 44]. Target compounds **5a-h** were obtained by acylation of hydantoins **3a-c** [44] with 5-(chloromethyl)-1,2,4-oxadiazole **4** [45, 46] and (5-oxopyrrolidin-3-yl)methyl mesylate **6** [47, 48] derivatives in DMF using $NaHCO_3$ as a base, which significantly reduced the formation of the dialkylation by-products [49].

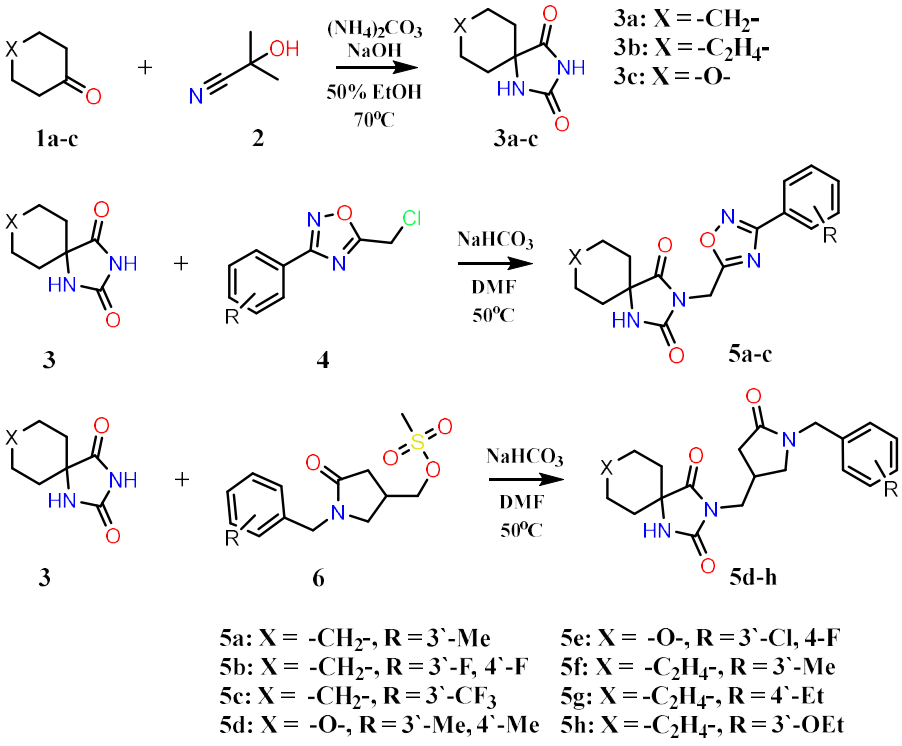

Fig. 11. Scheme for the synthesis of hydantoin derivatives (**5a-h**)

*General Procedure for synthesis of spyrohydantoins **3a-c**.*

Ammonium carbonate (25 mmol) was added to a solution of the corresponding ketone (1**a-c**) (10 mmol), and sodium hydroxide (15 mmol) in 50% EtOH (50 mL) and the mixture was stirred at rt for 30 min. Then, acetone cyanohydrin **2** (15 mmol) was added dropwise, and the reaction mixture was heated to 70°C. The resulting mixture was stirred for 12 h at 70°C, cooled to rt and diluted with water (40 mL). The reaction mixture was acidified with 1M HCl to pH 2. The formed precipitate was filtered off, washed with water and recrystallized from distilled water to get pure **3a-c** in 68–89% yield.

*1,3-Diazaspiro[4.5]decane-2,4-dione (**3a**).*

White crystals, *mp* = 216°C, 68% yield. ^{1}H NMR (400 MHz, DMSO-d_6) δ 10.50 (*s*, 1H), 8.37 (*s*, 1H), 1.63 (*m*, 1H), 1.62–1.55 (*m*, 3H), 1.49 (*m*, 5H), 1.31–1.18 (*m*, 1H).. $[MH]^+$ m/z = 169.3.

*1,3-Diazaspiro[4.6]undecane-2,4-dione (**3b**).*

White crystals, *mp* = 225°C, 73% yield. ^{1}H NMR (400 MHz, DMSO-d_6) δ 10.45 (*s*, 1H), 8.24–8.19 (*m*, 1H), 1.79 (*dt*, *J* = 9.6, 6.9 Hz, 2H), 1.65–1.48 (*m*, 10H). $[MH]^+$ m/z = 183.0.

8-*Oxa*-1,3-*diazaspiro*[4.5]*decane*-2,4-*dione (**3c**).*

White crystals, *mp* = 266°C, 89% yield. ^{1}H NMR (400 MHz, DMSO-*d*6) δ 10.66 (*s*, 1H), 8.57 (*s*, 1H), 3.80 (*dt*, *J* = 11.8, 4.2 Hz, 2H), 3.60 (*ddd*, *J* = 11.7, 10.7, 2.7 Hz, 2H), 1.83 (*ddd*, *J* = 13.5, 10.8, 4.6 Hz, 2H), 1.52–1.43 (*m*, 2H). $[MH]^+$ m/z = 177.1.

*General Procedure for alkylation of spirohydantoins **3a-c**.*

$NaHCO_3$ (3 mmol) was added to a solution of the corresponding spirohydantoine (**3a-c**) (1 mmol) in anhydrous DMF (10 mL), and the mixture was stirred at rt for 30 min. Then the reaction mixture was heated to 50°C and the corresponding alkylator (**4, 6**) (1.2 mmol) was slowly added. The resulting mixture was stirred for 3 h at 50°C, cooled to rt and diluted with water (40 mL). The formed precipitate was filtered off, washed with water and recrystallized from i-PrOH to get pure **5a-h** in 78–92% yield.

3-((3-(M-tolyl)-1,2,4-oxadiazol-5-yl)methyl)-1,3-diazaspiro [4.5]decane-2,4-dione (5a).

White powder, *mp* > 300°C, 92% yield. ^{1}H NMR (400 MHz, DMSO-d_6) δ 9.00 (*s*, 1H), 7.81–7.72 (*m*, 2H), 7.49–7.38 (m, 2H), 4.98 (*s*, 2H), 2.39 (*s*, 3H), 1.78–1.66 (*m*, 4H), 1.58 (*d*, *J* = 14.0 Hz, 4H), 1.52 (*d*, *J* = 12.7 Hz, 1H), 1.31 (*d*, *J* = 11.5 Hz, 1H). $[MH]^+$ m/z = 341.1.

3-((3-(3,4-*Difluorophenyl*)-1,2,4-*oxadiazol*-5-*yl*) *methyl*)-1,3-*diazaspiro*[4.5] *decane*-2,4-*dione (**5b**).*

White powder, *mp* > 300°C, 89% yield. ^{1}H NMR (400 MHz, DMSO-d_6) δ 9.01 (*s*, 1H), 7.96 (*ddd*, *J* = 11.1, 7.7, 2.1 Hz, 1H), 7.84 (*ddt*, *J* = 7.9, 4.4, 1.7 Hz, 1H), 7.66

(*dt*, *J* = 10.5, 8.4 Hz, 1H), 5.00 (*s*, 2H), 1.72 (*dd*, *J* = 14.4, 10.6 Hz, 2H), 1.68 (*s*, 1H), 1.62–1.47 (m, 6H), 1.32 (*t*, *J* = 11.7 Hz, 1H). $[MH]^+$ m/z = 363.2.

3-((3-(3-(Trifluoromethyl)phenyl)-1,2,4-oxadiazol-5-yl)methyl)-1,3-diazaspiro [4.5]decane-2,4-dione (5c).

White powder, *mp* > 300°C, 81% yield. ^{1}H NMR (400 MHz, DMSO-d_6) δ 9.01 (*s*, 1H), 8.27 (*d*, *J* = 7.9 Hz, 1H), 8.19 (*d*, *J* = 2.2 Hz, 1H), 8.00 (*d*, *J* = 7.9 Hz, 1H), 7.84 (*t*, *J* = 7.8 Hz, 1H), 5.02 (*s*, 2H), 1.79–1.65 (*m*, 4H), 1.57 (*t*, *J* = 14.3 Hz, 5H), 1.31 (*d*, *J* = 11.8 Hz, 1H). $[MH]^+$ m/z = 395.2.

3-((1-(3,4-*Dimethylbenzyl*)-5-*oxopyrrolidin*-3-*yl*) *methyl*)-8-*oxa*-1,3-*diazaspiro* [4.5]*decane*-2,4-*dione* (***5d***).

White powder, *mp* > 300°C, 78% yield. ^{1}H NMR (400 MHz, DMSO-d_6) δ 8.78 (*s*, 1H), 7.13–7.06 (*m*, 1H), 7.05–6.96 (*m*, 2H), 4.49 (*dt*, *J* = 12.3, 1.0 Hz, 1H), 4.41 (*dt*, *J* = 12.3, 1.0 Hz, 1H), 4.18 (*dd*, *J* = 12.5, 4.8 Hz, 1H), 3.90–3.78 (*m*, 2H), 3.70–3.48 (*m*, 5H), 2.66–2.48 (*m*, 2H), 2.37 (*ddt*, *J* = 14.4, 6.4, 3.1 Hz, 3H), 2.24 (*d*, *J* = 1.0 Hz, 3H), 2.20 (*s*, 3H), 2.02 (*d*, *J* = 14.6, 6.4, 3.7 Hz, 2H). $[MH]^+$ m/z = 386.2.

3-((1-(3-Chloro-4-fluorobenzyl)-5-oxopyrrolidin-3-yl) methyl)-8-oxa-1,3-diazaspiro[4.5]decane-2,4-dione (5e).

White powder, *mp* > 300°C, 80% yield. ^{1}H NMR (400 MHz, DMSO-d_6) δ 8.90 (*s*, 1H), 7.46–7.33 (*m*, 2H), 7.22 (*ddd*, *J* = 8.1, 4.8, 2.1 Hz, 1H), 4.36 (*d*, *J* = 15.1 Hz, 1H), 4.28 (*d*, *J* = 15.2 Hz, 1H), 3.81 (*dt*, *J* = 11.7, 4.3 Hz, 2H), 3.66–3.55 (m, 2H), 3.47–3.37 (*m*, 2H), 3.03 (*dd*, *J* = 9.9, 5.3 Hz, 1H), 2.63 (*dd*, *J* = 14.6, 7.3 Hz, 1H), 2.43 (*dd*, *J* = 16.7, 8.9 Hz, 1H), 2.12 (*dd*, *J* = 16.7, 6.3 Hz, 1H), 1.90–1.78 (*m*, 2H), 1.48 (*d*, *J* = 13.5 Hz, 2H), 1.24 (*d*, *J* = 9.9 Hz, 1H). $[MH]^+$ m/z = 410.2.

3-((1-(3-*Methylbenzyl*)-5-*oxopyrrolidin*-3-*yl*) *methyl*)-1,3-*diazaspiro*[4.6] *undecane*-2,4-*dione* (***5f***).

White powder, *mp* > 300°C, 82% yield. ^{1}H NMR (400 MHz, DMSO-d_6) δ 8.98 (*s*, 1H), 7.27–7.12 (*m*, 3H), 7.11–7.04 (*m*, 1H), 4.50 – 4.42 (*m*, 1H), 4.42–4.34 (*m*, 1H), 4.18 (*dd*, *J* = 12.5, 4.8 Hz, 1H), 3.90–3.78 (*m*, 2H), 3.57 (*dd*, *J* = 11.3, 4.4 Hz, 1H), 2.66–2.48 (*m*, 2H), 2.36 (*dd*, *J* = 14.5, 6.3 Hz, 1H), 2.29 (*s*, 3H), 1.85–1.73 (*m*, 2H), 1.61–1.31 (*m*, 10H). $[MH]^+$ m/z = 383.2.

3-((1-(4-*Ethylbenzyl*)-5-*oxopyrrolidin*-3-*yl*)*methyl*)-1,3-*diazaspiro*[4.6]*undecane*-2,4-*dione* (***5g***).

White powder, *mp* > 300°C, 84% yield. ^{1}H NMR (400 MHz, DMSO-*d*6) δ 8.91 (*s*, 1H), 7.23 (*dt*, *J* = 8.0, 0.9 Hz, 2H), 7.15 (*dt*, *J* = 8.2, 1.0 Hz, 2H), 4.50 (*dt*, *J* = 12.6, 1.0 Hz, 1H), 4.46–4.38 (*m*, 1H), 4.18 (*dd*, *J* = 12.5, 4.8 Hz, 1H), 3.90–3.78 (*m*, 2H), 3.57 (*dd*, *J* = 11.3, 4.4 Hz, 1H), 2.66–2.57 (*m*, 3H), 2.57–2.48 (*m*, 1H), 2.36 (*dd*, *J* = 14.5, 6.3 Hz, 1H), 1.85–1.73 (*m*, 2H), 1.59–1.31 (*m*, 10H), 1.20 (*t*, *J* = 7.2 Hz, 3H). $[MH]^+$ m/z = 397.2.

3-((1-(3-*Ethoxybenzyl*)-5-*oxopyrrolidin*-3-*yl*) *methyl*)-1,3-*diazaspiro*[4.6] *undecane*-2,4-*dione* (***5h***).

White powder, *mp* > 300°C, 86% yield. ^{1}H 1H NMR (400 MHz, DMSO-*d*6) δ 8.81 (*s*, 1H), 7.23 (*t*, *J* = 8.1 Hz, 1H), 7.11 (*dd*, *J* = 8.3, 2.1, 1H), 6.95–6.88 (*m*, 1H), 6.85 (*td*, *J* = 2.1, 1.0 Hz, 1H), 4.52 (*dt*, *J* = 12.3, 1.0 Hz, 1H), 4.45 (*dt*, *J* = 12.5, 1.0 Hz, 1H), 4.18 (*dd*, *J* = 12.5, 4.8 Hz, 1H), 4.05 (*q*, *J* = 6.7 Hz, 2H), 3.90–3.78 (*m*, 2H), 3.57 (*dd*, *J* = 11.2, 4.4 Hz, 1H), 2.66–2.48 (*m*, 2H), 2.36 (*dd*, *J* = 14.5, 6.3 Hz, 1H), 1.85–1.73 (*m*, 2H), 1.66–1.55 (*m*, 2H), 1.57–1.37 (*m*, 8H), 1.35 (*t*, *J* = 6.7 Hz, 3H). $[MH]^+$ m/z = 413.2.

5. Discussion of research results

The SARS-CoV-2 coronavirus relies on two vital proteases – the main protease M^{pro} and the papain-like protease PL^{pro} – for its replication within host cells [1]. Targeting these proteases has emerged as a promising strategy in the fight against COVID-19, with the potential of developing antiviral drugs that can effectively inhibit both enzymes capturing significant interest.

An innovative approach is presented for creating new peptidomimetic molecules that serve as dual-action inhibitors of both SARS-CoV-2 M^{pro} and PL^{pro} [7, 32]. Our research not only showcases the synthesis of these compounds but also highlights a thorough *in silico* evaluation process. We began by constructing a robust molecular model focused on the substrate specificity of each protease's active site. Through this strategic and rational design process, we identified a series of promising peptidomimetics. Moreover, our detailed analysis of the binding interactions between these compounds and the active sites of both proteases has led us to discover several new structural candidates, including hydantoin derivatives, which hold significant promise as dual inhibitors. This groundbreaking work paves the way for more effective therapeutic agents in the fight against SARS-CoV-2, showing great potential in mitigating the impact of this virus on public health.

We focused on analyzing the substrate specificity of the binding sites of the M^{pro} and PL^{pro} proteases, which led us to identify a common amino acid sequence that includes shared recognition elements for both enzymes. By thoughtfully modifying the functional groups in this foundational structure and applying the principles of isosteric replacement alongside non-classical bioisosteres, we successfully developed a series of innovative peptidomimetic frameworks. Our molecular docking studies at the active sites of both M^{pro} and PL^{pro}, combined with an evaluation of their binding affinity energy (Table 2), uncovered several promising structures with significant potential for dual inhibition. Notably, we found that hydantoin derivatives displayed the highest binding affinity to the active sites of both proteases, highlighting their potential for further development. Additionally, two derivatives, **5*f*** and **5*g*** (Fig. 11) revealed promising drug-like pharmacokinetic parameters (Table 3).

Practical relevance. The use of peptidomimetics as inhibitors for the main M^{pro} and papain-like PL^{pro} proteases of SARS-CoV-2 presents several significant advantages over natural peptide substrates or simple peptide inhibitors. Natural peptides are quickly degraded by viral proteases, resulting in a short half-life and poor bioavailability.

The practical relevance of our study is that the proposed peptidomimetics incorporate non-natural amino acids and modified peptide bonds, which enhance their resistance to enzymatic cleavage. The practical significance of these structural modifications is essential as it leads to greater stability of the inhibitors, translating

into a longer half-life in the body. Consequently, the drug can maintain therapeutic concentrations for an extended period, resulting in improved efficacy and potentially reducing the frequency of dosing.

Study limitations. The antiviral activity for the synthesized hydantoin derivatives has not been evaluated yet. Therefore, the potential therapeutic effect of the selected derivatives is only based on theoretical predictions.

Prospects for further research. The newly discovered hydantoin derivatives show potential for inhibiting both M^{pro} and PL^{pro} proteases, establishing them as a new class of dual-action agents. The developed retrosynthetic protocols will be further utilized to obtain additional derivatives for experimental *in vitro* studies.

6. Conclusion

The development of effective inhibitors for SARS-CoV-2 proteases is a critical priority in the search for anti-coronavirus agents. Designing new molecules that can target the active sites of both the M^{pro} and PL^{pro} proteases may reduce the chance of resistance and enhance the effectiveness of antiviral treatments [7]. In this study, we identified promising peptidomimetic molecular structures with dual inhibitory activity against SARS-CoV-2 proteases through *in silico* modelling. We discovered a new class of hydantoin derivatives that have the potential to inhibit both M^{pro} and PL^{pro} proteases. The synthesis methods we developed enabled us to obtain these compounds for further experimental *in vitro* studies.

Conflict of interest

The authors declare that they have no conflict of interest in relation to this research, whether financial, personal, authorship or otherwise, that could affect the research and its results presented in this article.

Funding

Grant No. 96/0062 (2021.01/0062) “Molecular design, synthesis and screening of new potential antiviral pharmaceutical ingredients for the treatment of infectious diseases COVID-19” from the National Research Foundation of Ukraine.

Data availability

The manuscript has no associated data.

Use of artificial intelligence

The authors confirm that they did not use artificial intelligence technologies when creating the current work.

Acknowledgments

We thank Prof. T. Langer for giving us the opportunity to utilize the LigandScout 4.5 suite.

Authors’ contributions

Pavlo Trostianko, Investigation, Formal analysis, Data curation**. Larysa Yevsieieva:** Conceptualization, Validation, Writing – review & editing, Writing – original draft, Methodology. **Alexander Kyrychenko:** Conceptualization, Validation, Writing – review & editing, Writing – original draft, Methodology. **Volodymyr Ivanov:** Conceptualization, Methodology, Writing – review & editing. **Sergiy M. Kovalenko:** Conceptualization, Supervision, Writing – review & editing. **Oleg Kalugin:** Conceptualization, Supervision, Project administration, Funding acquisition.

References

1. Yevsieieva, L. V., Lohachova, K. O., Kyrychenko, A., Kovalenko, S. M., Ivanov, V. V., Kalugin, O. N. (2023). Main and papain-like proteases as prospective targets for pharmacological treatment of coronavirus SARS-CoV-2. RSC Advances, 13 (50), 35500–35524. https://doi.org/10.1039/d3ra06479d

2. Capasso, C., Nocentini, A., Supuran, C. T. (2020). Protease inhibitors targeting the main protease and papain-like protease of coronaviruses. Expert Opinion on Therapeutic Patents, 31 (4), 309–324. https://doi.org/10.1080/13543776.2021.1857726

3. Wang, Y., Xu, B., Ma, S., Wang, H., Shang, L., Zhu, C., Ye, S. (2022). Discovery of SARS-CoV-2 3CLPro Peptidomimetic Inhibitors through the Catalytic Dyad Histidine-Specific Protein-Ligand Interactions. International Journal of Molecular Sciences, 23 (4), 2392. https://doi.org/10.3390/ijms23042392

4. Kerti, L., Frecer, V. (2024). Design of inhibitors of SARS-CoV-2 papain-like protease deriving from GRL0617: Structure–activity relationships. Bioorganic & Medicinal Chemistry, 113, 117909. https://doi.org/10.1016/j.bmc.2024.117909

5. Lohachova, K. O., Kyrychenko, A., Kalugin, O. N. (2025). Benchmarking biomolecular force fields for molecular dynamics simulations of native fold and enzymatic activity of SARS-CoV-2 papain-like protease. Heliyon, 11 (12), e43578. https://doi.org/10.1016/j.heliyon.2025.e43578

6. Garnsey, M. R., Robinson, M. C., Nguyen, L. T., Cardin, R., Tillotson, J., Mashalidis, E. et al. (2024). Discovery of SARS-CoV-2 papain-like protease (PLpro) inhibitors with efficacy in a murine infection model. bioRxiv. https://doi.org/10.1101/2024.01.26.577395

7. Yevsieieva, L., Trostianko, P., Kyrychenko, A., Ivanov, V., Kovalenko, S., Kalugin, O. (2024). Design of non-covalent dual-acting inhibitors for proteases M^{PRO} and PL^{PRO} of coronavirus SARS-CoV-2 through evolutionary library generation, pharmacophore profile matching, and molecular docking calculations. ScienceRise: Pharmaceutical Science, 6 (52), 15–26. https://doi.org/10.15587/2519-4852.2024.313808

8. Ma, C., Sacco, M. D., Xia, Z., Lambrinidis, G., Townsend, J. A., Hu, Y. et al. (2021). Discovery of SARS-CoV-2 Papain-like Protease Inhibitors through a Combination of High-Throughput Screening and a FlipGFP-Based Reporter Assay. ACS Central Science, 7 (7), 1245–1260. https://doi.org/10.1021/acscentsci.1c00519

9. Lucas, S. C. C., Blackwell, J. H., Hewitt, S. H., Semple, H., Whitehurst, B. C., Xu, H. (2024). Covalent hits and where to find them. SLAS Discovery, 29 (3), 100142. https://doi.org/10.1016/j.slasd.2024.01.003

10. Ivanov, V., Lohachova, K., Kolesnik, Y., Zakharov, A., Yevsieieva, L., Kyrychenko, A. et al. (2023). Recent advances in computational drug discovery for therapy against coronavirus SARS-CoV-2. ScienceRise: Pharmaceutical Science, 6 (46), 4–24. https://doi.org/10.15587/2519-4852.2023.290318

11. Zhang, L., Lin, D., Sun, X., Curth, U., Drosten, C., Sauerhering, L. et al. (2020). Crystal structure of SARS-CoV-2 main protease provides a basis for design of improved α-ketoamide inhibitors. Science, 368 (6489), 409–412. https://doi.org/10.1126/science.abb3405

12. Xia, Z., Sacco, M., Hu, Y., Ma, C., Meng, X., Zhang, F. et al. (2021). Rational Design of Hybrid SARS-CoV-2 Main Protease Inhibitors Guided by the Superimposed Cocrystal Structures with the Peptidomimetic Inhibitors GC-376, Telaprevir, and Boceprevir. ACS Pharmacology & Translational Science, 4 (4), 1408–1421. https://doi.org/10.1021/acsptsci.1c00099

13. Citarella, A., Scala, A., Piperno, A., Micale, N. (2021). SARS-CoV-2 Mpro: A Potential Target for Peptidomimetics and Small-Molecule Inhibitors. Biomolecules, 11 (4), 607. https://doi.org/10.3390/biom11040607

14. Bege, M., Borbás, A. (2024). The Design, Synthesis and Mechanism of Action of Paxlovid, a Protease Inhibitor Drug Combination for the Treatment of COVID-19. Pharmaceutics, 16 (2), 217. https://doi.org/10.3390/pharmaceutics16020217

15. Lohachova, K. O., Sviatenko, A. S., Kyrychenko, A., Ivanov, V. V., Langer, T., Kovalenko, S. M., Kalugin, O. N. (2024). Computer-aided drug design of novel nirmatrelvir analogs inhibiting main protease of Coronavirus SARS-CoV-2. Journal of Applied Pharmaceutical Science, 14 (5), 232–239. https://doi.org/10.7324/japs.2024.158114

16. Arafet, K., Serrano-Aparicio, N., Lodola, A., Mulholland, A. J., González, F. V., Świderek, K., Moliner, V. (2021). Mechanism of inhibition of SARS-CoV-2 Mpro by N3 peptidyl Michael acceptor explained by QM/MM simulations and design of new derivatives with tunable chemical reactivity. Chemical Science, 12 (4), 1433–1444. https://doi.org/10.1039/d0sc06195f

17. Bauer, R. A. (2015). Covalent inhibitors in drug discovery: from accidental discoveries to avoided liabilities and designed therapies. Drug Discovery Today, 20 (9), 1061–1073. https://doi.org/10.1016/j.drudis.2015.05.005

18. Singh, J., Petter, R. C., Baillie, T. A., Whitty, A. (2011). The resurgence of covalent drugs. Nature Reviews Drug Discovery, 10 (4), 307–317. https://doi.org/10.1038/nrd3410

19. Schaefer, D., Cheng, X. (2023). Recent Advances in Covalent Drug Discovery. Pharmaceuticals, 16 (5), 663. https://doi.org/10.3390/ph16050663

20. Hu, Y., Ma, C., Szeto, T., Hurst, B., Tarbet, B., Wang, J. (2021). Boceprevir, Calpain Inhibitors II and XII, and GC-376 Have Broad-Spectrum Antiviral Activity against Coronaviruses. ACS Infectious Diseases, 7 (3), 586–597. https://doi.org/10.1021/acsinfecdis.0c00761

21. Kneller, D. W., Li, H., Phillips, G., Weiss, K. L., Zhang, Q., Arnould, M. A. et al. (2022). Covalent narlaprevir- and boceprevir-derived hybrid inhibitors of SARS-CoV-2 main protease. Nature Communications, 13 (1), 2268. https://doi.org/10.1038/s41467-022-29915-z

22. Joyce, R. P., Hu, V. W., Wang, J. (2022). The history, mechanism, and perspectives of nirmatrelvir (PF-07321332): an orally bioavailable main protease inhibitor used in combination with ritonavir to reduce COVID-19-related hospitalizations. Medicinal Chemistry Research, 31 (10), 1637–1646. https://doi.org/10.1007/s00044-022-02951-6

23. Tan, H., Hu, Y., Jadhav, P., Tan, B., Wang, J. (2022). Progress and Challenges in Targeting the SARS-CoV-2 Papain-like Protease. Journal of Medicinal Chemistry, 65 (11), 7561–7580. https://doi.org/10.1021/acs.jmedchem.2c00303

24. Osipiuk, J., Azizi, S.-A., Dvorkin, S., Endres, M., Jedrzejczak, R., Jones, K. A. et al. (2021). Structure of papain-like protease from SARS-CoV-2 and its complexes with non-covalent inhibitors. Nature Communications, 12 (1), 743. https://doi.org/10.1038/s41467-021-21060-3

25. Ton, A.-T., Pandey, M., Smith, J. R., Ban, F., Fernandez, M., Cherkasov, A. (2022). Targeting SARS-CoV-2 papain-like protease in the postvaccine era. Trends in Pharmacological Sciences, 43 (11), 906–919. https://doi.org/10.1016/j.tips.2022.08.008

26. Rut, W., Lv, Z., Zmudzinski, M., Patchett, S., Nayak, D., Snipas, S. J. et al. (2020). Activity profiling and crystal structures of inhibitor-bound SARS-CoV-2 papain-like protease: A framework for anti–COVID-19 drug design. Science Advances, 6 (42), eabd4596. https://doi.org/10.1126/sciadv.abd4596

27. Gao, X., Qin, B., Chen, P., Zhu, K., Hou, P., Wojdyla, J. A., Wang, M., Cui, S. (2021). Crystal structure of SARS-CoV-2 papain-like protease. Acta Pharmaceutica Sinica B, 11 (1), 237–245. https://doi.org/10.1016/j.apsb.2020.08.014

28. Ullrich, S., Nitsche, C. (2022). SARS-CoV-2 Papain-Like Protease: Structure, Function and Inhibition. ChemBioChem, 23 (19). https://doi.org/10.1002/cbic.202200327

29. Yuan, S., Gao, X., Tang, K., Cai, J.-P., Hu, M., Luo, P. et al. (2022). Targeting papain-like protease for broad-spectrum coronavirus inhibition. Protein & Cell, 13 (12), 940–953. https://doi.org/10.1007/s13238-022-00909-3

30. Wang, Q., Chen, G., He, J., Li, J., Xiong, M., Su, H. et al. (2023). Structure-Based Design of Potent Peptidomimetic Inhibitors Covalently Targeting SARS-CoV-2 Papain-like Protease. International Journal of Molecular Sciences, 24 (10), 8633. https://doi.org/10.3390/ijms24108633

31. Yu, W., Zhao, Y., Ye, H., Wu, N., Liao, Y., Chen, N. et al. (2022). Structure-Based Design of a Dual-Targeted Covalent Inhibitor Against Papain-like and Main Proteases of SARS-CoV-2. Journal of Medicinal Chemistry, 65 (24), 16252–16267. https://doi.org/10.1021/acs.jmedchem.2c00954

32. Santos, L. H., Kronenberger, T., Almeida, R. G., Silva, E. B., Rocha, R. E. O., Oliveira, J. C. et al. (2022). Structure-Based Identification of Naphthoquinones and Derivatives as Novel Inhibitors of Main Protease Mpro and Papain-like Protease PLpro of SARS-CoV-2. Journal of Chemical Information and Modeling, 62 (24), 6553–6573. https://doi.org/10.1021/acs.jcim.2c00693

33. Reddy, A. S., Zhang, S. (2013). Polypharmacology: drug discovery for the future. Expert Review of Clinical Pharmacology, 6 (1), 41–47. https://doi.org/10.1586/ecp.12.74

34. Sander, T., Freyss, J., von Korff, M., Rufener, C. (2015). DataWarrior: An Open-Source Program For Chemistry Aware Data Visualization And Analysis. Journal of Chemical Information and Modeling, 55 (2), 460–473. https://doi.org/10.1021/ci500588j

35. Wolber, G., Langer, T. (2005). LigandScout: 3-D Pharmacophores Derived from Protein-Bound Ligands and Their Use as Virtual Screening Filters. Journal of Chemical Information and Modeling, 45 (1), 160–169. https://doi.org/10.1021/ci049885e

36. Goodsell, D. S., Morris, G. M., Olson, A. J. (1996). Automated docking of flexible ligands: Applications of AutoDock. Journal of Molecular Recognition, 9(1), 1–5. https://doi.org/10.1002/(sici)1099-1352(199601)9:1<1::aid-jmr241>3.0.co;2-6

37. Goodsell, D. S., Sanner, M. F., Olson, A. J., Forli, S. (2020). The AutoDock suite at 30. Protein Science, 30 (1), 31–43. https://doi.org/10.1002/pro.3934

38. Kumar, T. D. A. (2022). Drug Design. A Conceptual Overview. Abingdon: CRC Press. https://doi.org/10.1201/9781003298755

39. La Monica, G., Bono, A., Lauria, A., Martorana, A. (2022). Targeting SARS-CoV-2 Main Protease for Treatment of COVID-19: Covalent Inhibitors Structure-Activity Relationship Insights and Evolution Perspectives. Journal of Medicinal Chemistry, 65 (19), 12500–12534. https://doi.org/10.1021/acs.jmedchem.2c01005

40. Bucherer, H. Th., Lieb, V. A. (1934). Über die Bildung substituierter Hydantoine aus Aldehyden und Ketonen. Synthese von Hydantoinen. Journal Für Praktische Chemie, 141 (1-2), 5–43. https://doi.org/10.1002/prac.19341410102

41. Konnert, L., Lamaty, F., Martinez, J., Colacino, E. (2017). Recent Advances in the Synthesis of Hydantoins: The State of the Art of a Valuable Scaffold. Chemical Reviews, 117 (23), 13757–13809. https://doi.org/10.1021/acs.chemrev.7b00067

42. Kalník, M., Gabko, P., Bella, M., Koóš, M. (2021). The Bucherer-Bergs Multicomponent Synthesis of Hydantoins – Excellence in Simplicity. Molecules, 26 (13), 4024. https://doi.org/10.3390/molecules26134024

43. Park, E. J., Lee, S., Chang, S. (2010). Acetone Cyanohydrin as a Source of HCN in the Cu-Catalyzed Hydrocyanation of α-Aryl Diazoacetates. The Journal of Organic Chemistry, 75 (8), 2760–2762. https://doi.org/10.1021/jo100356d

44. Cho, S., Kim, S.-H., Shin, D. (2019). Recent applications of hydantoin and thiohydantoin in medicinal chemistry. European Journal of Medicinal Chemistry, 164, 517–545. https://doi.org/10.1016/j.ejmech.2018.12.066

45. Ölmez, N. A., Waseer, F. (2020). New Potential Biologically Active Compounds: Synthesis and Characterization of Urea and Thiourea Derivativpes Bearing 1,2,4-oxadiazole Ring. Current Organic Synthesis, 17 (7), 525–534. https://doi.org/10.2174/1570179417666200417112106

46. Zhu, L., Zeng, H., Liu, D., Fu, Y., Wu, Q., Song, B., Gan, X. (2020). Design, synthesis, and biological activity of novel 1,2,4-oxadiazole derivatives. BMC Chemistry, 14 (1), 68. https://doi.org/10.1186/s13065-020-00722-1

47. Perekhoda, L., Suleiman, M., Podolsky, I., Semenets, A., Kobzar, N., Yaremenko, V. et al. (2024). Synthesis and nootropic activity prediction of some 4-(aminomethyl)-1-benzylpyrrolidin-2-one derivatives structurally related with nebracetam. ScienceRise: Pharmaceutical Science, 4 (50), 23–34. https://doi.org/10.15587/2519-4852.2024.310731

48. Semenets, A. P., Suleiman, M. M., Fedosov, A. I., Shtrygol, S. Y., Havrylov, I. O., Mishchenko, M. V. et al. (2022). Synthesis, docking, and biological evaluation of novel 1-benzyl-4-(4-(R)-5-sulfonylidene-4,5-dihydro-1H-1,2,4-triazol-3-yl)pyrrolidin-2-ones as potential nootropic agents. European Journal of Medicinal Chemistry, 244, 114823. https://doi.org/10.1016/j.ejmech.2022.114823

49. Shintani, Y., Kato, K., Kawami, M., Takano, M., Kumamoto, T. (2021). Direct N1-Selective Alkylation of Hydantoins Using Potassium Bases. Chemical and Pharmaceutical Bulletin, 69 (4), 407–410. https://doi.org/10.1248/cpb.c20-00857

Received 27.08.2025
Received in revised form 13.10.2025
Accepted 22.10.2025
Published 27.10.2025

Larysa Yevsieieva, Senior Lecturer, Education and Research Institute of Chemistry, V. N. Karazin Kharkiv National University, Svobody sq., 4, Kharkiv, Ukraine, 61022

Alexander Kyrychenko*, Doctor of Chemical Sciences, Head of Department, Education and Research Institute of Chemistry, V. N. Karazin Kharkiv National University, Svobody sq., 4, Kharkiv, Ukraine, 61022

Pavlo Trostianko, PhD Student, Education and Research Institute of Chemistry, V. N. Karazin Kharkiv National University, Svobody sq., 4, Kharkiv, Ukraine, 61022

Volodymyr Ivanov, Doctor of Chemical Sciences, Professor, Education and Research Institute of Chemistry, V. N. Karazin Kharkiv National University, Svobody sq., 4, Kharkiv, Ukraine, 61022

Sergiy Kovalenko, Doctor of Chemical Sciences, Professor, Education and Research Institute of Chemistry, V. N. Karazin Kharkiv National University, Svobody sq., 4, Kharkiv, Ukraine, 61022

Oleg Kalugin, PhD, Professor, Education and Research Institute of Chemistry, V. N. Karazin Kharkiv National University, Svobody sq., 4, Kharkiv, Ukraine, 61022

***Corresponding author:** Alexander Kyrychenko, e-mail: a.v.kyrychenko@karazin.ua*